NASA Technical Paper 3100

May 1991

# Numerical Studies of Convective Cooling for a Locally Heated Skin

Stephen J. Scotti



NASA

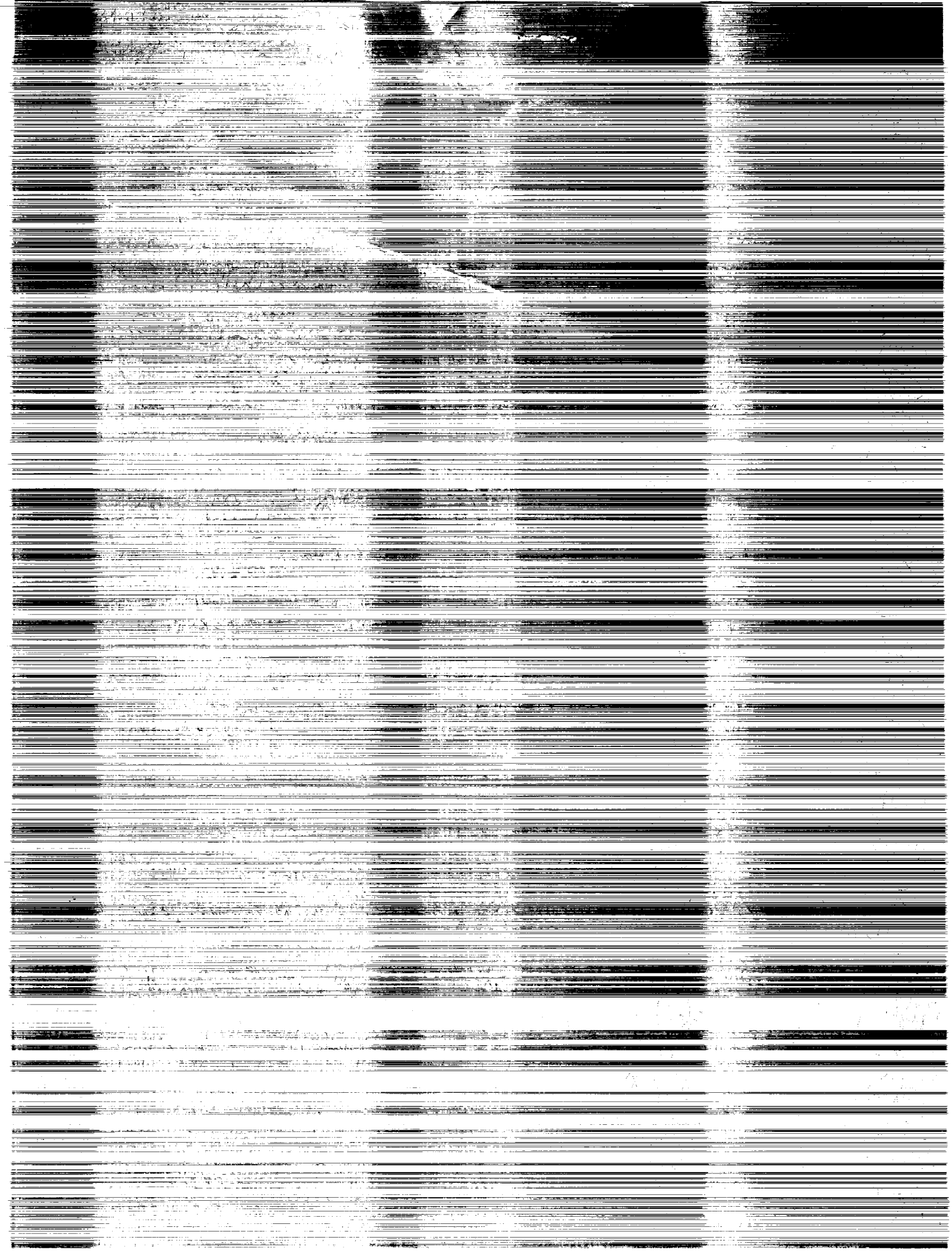

**NASA Technical Paper 3100**

1991

# Numerical Studies of Convective Cooling for a Locally Heated Skin

Stephen J. Scotti
*Langley Research Center*
*Hampton, Virginia*

National Aeronautics and Space Administration
Office of Management
Scientific and Technical Information Division

## Abstract

A computational study of the effectiveness of tangential convective cooling for the protection of structures from intense, localized thermal loads is presented. Two-dimensional numerical models of an idealized cooling problem are developed and validated. Detailed results and a parametric study of cooling effectiveness are presented for a thermal load representative of a shock-shock interaction on the engine cowl leading edge of a hypersonic study vehicle. The parameters investigated are flow conditions (laminar or turbulent), coolant type (liquid sodium, liquid water, or supercritical, cryogenic hydrogen), coolant mass-flow rate, extent of the heated region, thickness of the heated skin, and bulk properties of the coolant. The results indicate that for specific combinations of parameters, all three coolants may yield temperatures within the temperature limits of a copper-alloy, engine cowl leading edge. However, a liquid sodium coolant is the least sensitive of the three coolants to the assumed flow conditions and to the other parameters investigated in the study.

## Introduction

The capability of cooling structures and systems subjected to intense, localized thermal loads can be a significant design problem. As an example, the National Aero-Space Plane (NASP) is expected to operate at flight conditions that produce severe aerothermal heating of the engine cowl leading edge as a result of shock-shock interactions. (See ref. 1.) A schematic of this situation and the heat-flux distribution on the engine cowl leading edge is given in figure 1. Estimates of the amplification ($\approx 30\times$) of the undisturbed heating due to the interactions (ref. 2) predict a maximum heating rate of over 50 000 Btu/ft$^2$-sec.

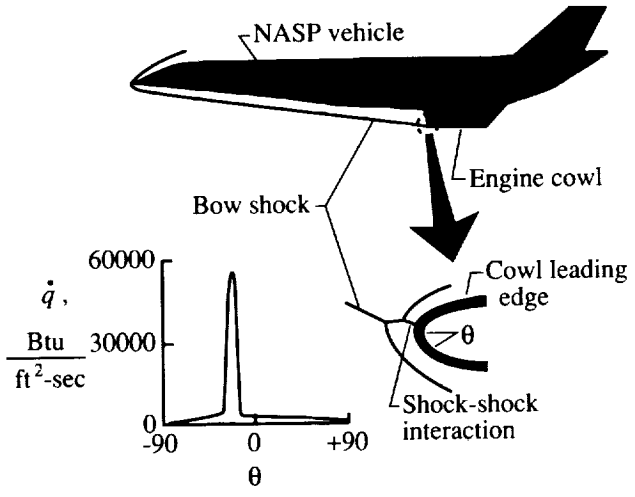


Figure 1. Schematic of a NASP vehicle and the heat-flux distribution on engine cowl leading edge.

The effectiveness of internal, tangential convective cooling for heating conditions that represent a shock-shock interaction on the engine cowl leading edge of a hypersonic vehicle is investigated in the present study. A two-dimensional analysis is performed in which the velocity profiles of the coolant are calculated for developing laminar and fully developed turbulent flows. Detailed results for temperatures, heat fluxes, and Nusselt numbers are presented for a typical case of a water-cooled skin subjected to this localized thermal load. The capabilities of liquid sodium, liquid water, and supercritical, cryogenic hydrogen for tangential convective cooling are examined in a parametric study that compares maximum skin temperature with variations of coolant mass-flow rate, extent of the heated region, skin thickness, and bulk properties.

## Symbols

| | |
|---|---|
| $A^+$ | Van Driest empirical constant, $\approx 26$ |
| Bi | Biot number (eq. (A6)) |
| $C$ | empirical constant, $\approx 0.2$ (eq. (18)) |
| $c_f$ | skin-friction coefficient for fully developed turbulent flow, $(2\nu/\bar{u}^2)\partial u/\partial y$ at $y = 0$ |
| $c_p$ | specific heat, Btu/lbm-°F |
| $D_h$ | hydraulic diameter, $2h_c$, ft |
| $h$ | height or thickness (dimension in $y$ direction), in. |
| $h_H$ | convective film coefficient, $\mathrm{Nu}k_c/D_h$, Btu/ft$^2$-sec-°F |
| $k$ | thermal conductivity, Btu/ft-sec-°F |
| $l$ | length before application of heat load, in. |
| Nu | Nusselt number (eq. (28)) |
| $\mathrm{Pe}_t$ | turbulent Péclet number, $\mathrm{Pr}\,\epsilon_M/\nu$ |
| $\mathrm{Pr}, \mathrm{Pr}_t$ | Prandtl number ($\nu/\alpha$) and turbulent Prandtl number ($\epsilon_M/\epsilon_H$) |
| $\mathrm{Pr}_{t_\infty}$ | empirical constant, $\approx$ 0.86 (eq. (18)) |
| $p$ | pressure, lbm/ft-sec$^2$ |
| $\dot{Q}$ | applied uniform heat flux, Btu/ft$^2$-sec |
| $\dot{q}$ | heat flux, Btu/ft$^2$-sec |
| $q_x^-, q_x^+, q_y^-, q_y^+$ | heat flows per unit depth near interface of coolant and skin (eqs. (23) to (27)), Btu/ft-sec |

| | |
|---|---|
| $R$ | Reynolds number, $\bar{u}D_h/\nu$ |
| $T$ | temperature, °F |
| $t$ | time, sec |
| $u, v$ | streamwise and cross-stream velocities, ft/sec |
| $\bar{u}$ | average streamwise velocity, ft/sec |
| $u^+$ | nondimensional "wall" velocity, $u/\bar{u}\sqrt{c_f/2}$ |
| $w$ | extent of applied uniform heat flux, in. |
| $x, y$ | streamwise and cross-stream coordinates, in. |
| $x^+$ | nondimensional streamwise coordinate $(x/D_h)/(R\,\mathrm{Pr})$ |
| $y^+$ | nondimensional wall coordinate, $y\bar{u}\sqrt{c_f/2}\,/\nu$ |
| $\alpha$ | molecular thermal diffusivity, $k/(\rho c_p)$, ft$^2$/sec |
| $\Delta T$ | temperature change over a time step (i.e., $\Delta T^n = T^{n+1} - T^n$) or change in maximum skin temperature from nominal analysis conditions (i.e., $\Delta T_s = T_{s,\max} - T_{s,\max,\mathrm{nom}}$), °F |
| $\Delta t$ | time step, sec |
| $\Delta x$ | $x$-direction step used in finite-difference analogs, ft |
| $\Delta y$ | $y$-direction step used in finite-difference analogs, ft |
| $\epsilon_H, \epsilon_M$ | eddy diffusivity for heat transfer and momentum, ft$^2$/sec |
| $\kappa$ | turbulent mixing-length constant, $\approx 0.4$ |
| $\mu$ | viscosity, lbm/ft-sec |
| $\nu$ | kinematic viscosity, $\mu/\rho$, ft$^2$/sec |
| $\rho$ | density, lbm/ft$^3$ |

Subscripts:

| | |
|---|---|
| $b$ | bulk coolant values |
| $c$ | coolant |
| $cl$ | centerline (i.e., $y_{cl} = h_c/2$) |
| $i$ | interface between skin and coolant (i.e., $y_i = 0$) |
| in | channel inlet (i.e., $x = 0$) |
| max | maximum |
| nom | nominal analysis conditions |
| $s$ | skin |

Superscripts:

| | |
|---|---|
| $c$ | core region of coolant |
| $i$ | $x$-coordinate location $i$ ($i$ increases for increasing $x$) |
| $j$ | $y$-coordinate location $j$ ($j$ increases for increasing $y$) |
| $n$ | time level (i.e., $t^n = n\Delta t$) |
| $w$ | wall region of coolant |
| $\prime$ | indicates bulk temperature used for determining properties |

## Leading-Edge Cooling Concepts

Several actively cooled concepts that have been proposed to accommodate the extreme heat rates on a cowl leading edge are shown in figure 2. These concepts for cooling the cowl leading edge include devices that combine a liquid-metal heat pipe and convective coolant flows, that transpire coolant through a porous metal surface, and that convectively cool using impingement or tangential coolant flows. All these methods have limitations when applied to cooling intense, localized heat fluxes that result from shock-shock interactions. Heat pipes are limited by boiling in the wick beneath the heated zone and by fluid flow limits related to the capillary pumping capability of the wick structure. Transpiration cooling may not be very effective in this application. Preliminary tests in reference 3 indicate only a small reduction in surface heating due to uniform transpiration cooling of a leading edge subjected to shock-shock interactions for transpiration flow rates that completely eliminate the undisturbed surface heating. Transpiration-cooled concepts may also be more susceptible to damage and blockage than other cooling methods because of a porous outer surface. Furthermore, since the shock-shock interaction is flow induced, it may be impossible to validate the capability of transpiration cooling because of the limitations of present wind-tunnel facilities. The main disadvantage of impingement cooling is that its high cooling effectiveness is localized, and thus the accurate prediction of the location of the localized thermal load is necessary.

One method that has not been adequately assessed for a cowl leading-edge application is tangential convective cooling, or channel flow cooling, of the heated

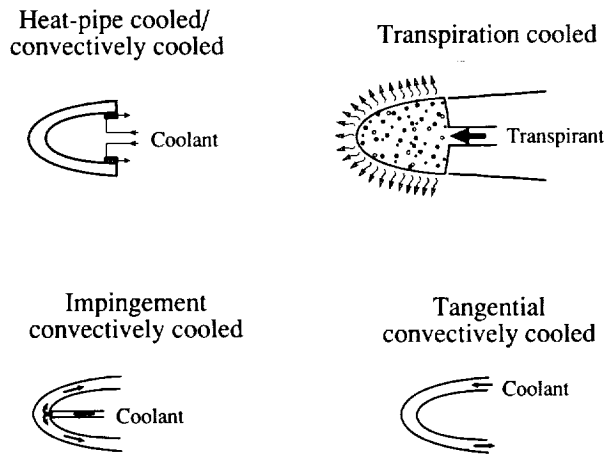


Figure 2. Several cooling concepts for a cowl leading edge.

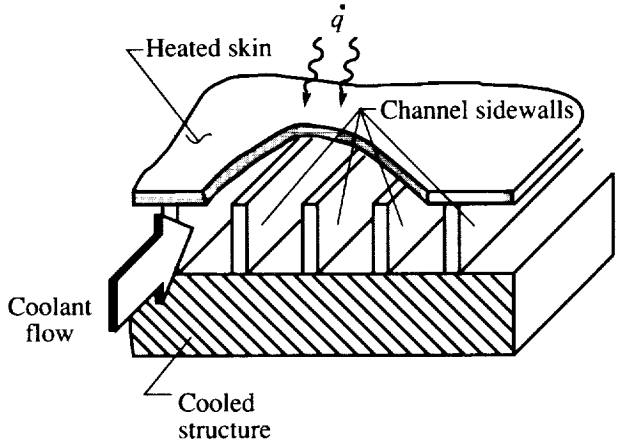


Figure 3. Channel-flow geometry for tangential convective cooling.

structure. In this method, coolant flows in channels between the heated skin and the cooled structure, which are connected by channel sidewalls as shown in figure 3. This convective cooling scheme is used for heat fluxes of over 14 000 Btu/ft$^2$-sec in the space shuttle main engine (ref. 4). However, tangential convective cooling can be effectively utilized for even higher heat fluxes when these high fluxes are localized. This is possible because the skin temperatures are reduced by two effects: the thinness of the thermal boundary layer, which effectively redevelops near a localized thermal load, and the lateral (streamwise) conduction in the heated skin. Experimental evidence of the former effect is presented in reference 5. In this reference, the Nusselt number at a coolant-skin interface (a measure of cooling effectiveness) increases 60 percent over that for a uniform heat flux due to the local nature of the thermal load. If the capability to cool high, localized heat fluxes can

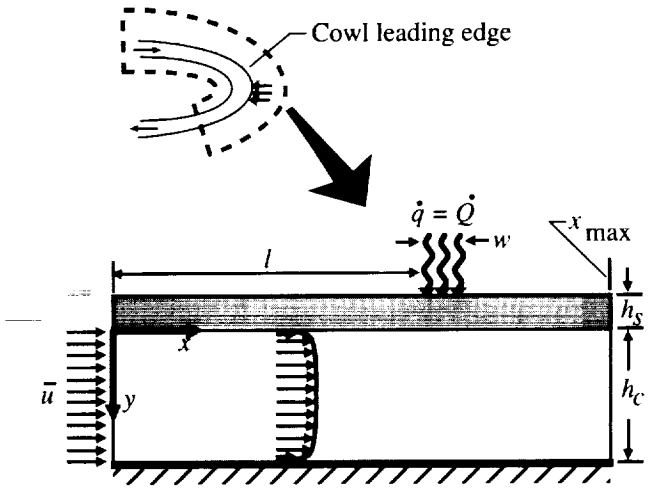


Figure 4. Schematic of geometry for convective cooling problem.

be demonstrated, tangential convective cooling is the preferred method because of its simplicity.

## Analysis

In this section, the governing equations, boundary conditions, and other assumptions for an idealized tangential convective cooling problem are described. The numerical algorithms that are used to solve the equations and the verification cases are also presented.

### Description of Problem

Figure 4 is a schematic of the idealized geometry in the convection-conduction problem of a cowl leading edge subjected to shock-shock interactions. In this idealization, the curvature of the cowl leading edge, as shown in the figure inset, is neglected. The conduction in the channel sidewalls (fig. 3) is ignored to make a two-dimensional analysis possible. Only the intense, localized heat flux due to the shock-shock interaction is considered. Also, the temperature dependence of material properties is ignored. These assumptions are made to simplify the solution of the problem. In figure 4, the coolant flows in a channel of height $h_c$, which is bounded above by the heated metallic skin with a thickness of $h_s$, and below by an insulated wall. A coordinate system is located in the figure with the $x$-axis in the flow direction and the $y$-axis in the cross-stream direction. The origin of the coordinate system is taken as the entrance to the channel at the interface between the coolant and the skin. In the laminar-flow cases, the coolant enters with the uniform velocity $\bar{u}$ as shown on the left of figure 4. This flow will develop symmetrically as shown in the schematic velocity profile. In the fully developed turbulent-flow

cases, the velocity profile shape is independent of the $x$-location. A steady, uniform heat flux ($\dot{q} = \dot{Q}$) is applied beginning at the location $x = l$ on the external face of the skin and extending for a length $w$. All other surfaces bounding the channel-skin system are insulated.

### Governing Equations

The equations that describe the physics of the convective cooling problem are the momentum, continuity, and energy equations of continuum mechanics. Steady, incompressible flow of a constant property coolant in the channel is assumed to simplify the solution of the problem. However, these assumptions may lead to inaccurate results in some cases, especially for the hydrogen coolant (a compressible fluid that undergoes large local temperature changes). The momentum and continuity equations for this two-dimensional flow are:

$$u\frac{\partial u}{\partial x} + v\frac{\partial u}{\partial y} = -\frac{1}{\rho}\frac{dp}{dx} + \frac{\partial}{\partial y}\left[(\nu + \epsilon_M)\frac{\partial u}{\partial y}\right] \tag{1}$$

$$\frac{\partial u}{\partial x} + \frac{\partial v}{\partial y} = 0 \tag{2}$$

where the thin-shear-layer form of the momentum equation is utilized. Although constant molecular transport and thermodynamic properties are assumed, the eddy diffusivity for momentum $\epsilon_M$ is contained within the derivatives because it is a function of the $y$ coordinate. The form of this eddy diffusivity is given subsequently. Because the velocities are symmetric about the centerline of the channel, only half the channel height is modeled, and the boundary conditions are as follows:

$$u = v = 0 \qquad (y = 0) \tag{3}$$

$$\frac{\partial u}{\partial y} = v = 0 \qquad (y = y_{cl}) \tag{4}$$

For the developing laminar-flow cases, the velocity profile for the coolant entering the channel at $x = 0$ must be given. In this study, a uniform profile is assumed as follows:

$$u(x = 0, y) = \bar{u} \qquad (0 < y \leq y_{cl}) \tag{5}$$

The energy equations for the coolant and the skin must be coupled and solved to determine temperatures. They are given in time-dependent form, because a transient-solution algorithm is used to integrate a time-varying temperature to steady state. This algorithm is described subsequently. The molecular transport and thermodynamic properties are assumed to be constant. The eddy diffusivity for heat transfer $\epsilon_H$ is assumed to be a function of the $y$ coordinate, and viscous dissipation of the fluid is neglected. The energy equations are

$$\frac{\partial T}{\partial t} + u\frac{\partial T}{\partial x} + v\frac{\partial T}{\partial y} = \alpha_c\frac{\partial^2 T}{\partial x^2} + \frac{\partial}{\partial y}\left[(\alpha_c + \epsilon_H)\frac{\partial T}{\partial y}\right] \qquad (y > 0) \tag{6}$$

and

$$\frac{\partial T}{\partial t} = \alpha_s\left(\frac{\partial^2 T}{\partial x^2} + \frac{\partial^2 T}{\partial y^2}\right) \qquad (y < 0) \tag{7}$$

where equation (6) is for the coolant and equation (7) is for the skin. The thin-shear-layer assumption, which removes the lateral diffusion term in the momentum equation (eq. (1)), is not made in the coolant energy equation (eq. (6)), because it is necessary to accommodate lateral conduction in the skin. The insulated wall boundary condition for the coolant is

$$\frac{\partial T}{\partial y} = 0 \qquad (y = h_c) \tag{8}$$

The boundary condition at the heated surface ($y = -h_s$) is

$$-k_s\frac{\partial T_s}{\partial y} = \begin{cases} \dot{Q} & (l \leq x \leq (l + w)) \\ 0 & \text{(Otherwise)} \end{cases} \tag{9}$$

At the coolant-skin interface ($y = 0$), the temperatures and the $y$-direction heat fluxes in the coolant and the skin must agree as follows:

$$T_s = T_c \tag{10}$$

$$k_s\frac{\partial T_s}{\partial y} = k_c\frac{\partial T_c}{\partial y} \tag{11}$$

To complete the boundary conditions for the energy equations, conditions on the temperature at the entrance and exit planes of the channel are given. At the entrance plane ($x = 0$), the conditions are

$$T = 0 \qquad (0 \leq y < h_c) \tag{12}$$

and

$$\frac{\partial T}{\partial x} = 0 \qquad (-h_s \leq y < 0) \tag{13}$$

Because the energy equations are linear in temperature and constant properties are used, the temperature of

the coolant entering the channel is set to zero; thus, the temperature rise is computed. The actual coolant inlet temperature $T_{\text{in}}$ may be added to the calculated temperature rise to obtain actual temperatures. At the exit plane ($x = x_{\max}$), the zero gradient condition is also used:

$$\frac{\partial T}{\partial x} = 0 \qquad (-h_s \le y \le h_c) \tag{14}$$

### Turbulence Models

The eddy diffusivity terms $\epsilon_M$ and $\epsilon_H$, which are nonzero only in the turbulent flow cases, are now defined. To make a simple solution for turbulent flow possible, the Reichardt (ref. 6) and Van Driest (ref. 7) empirical correlations, which have proven accurate for simple pipe flows, are employed. First, the skin-friction coefficient $c_f$ is obtained from an assumed average velocity $\bar{u}$ by utilizing the following relation developed by Petukhov (ref. 8):

$$c_f = \frac{2}{[2.236 \ln(R) - 4.639]^2} \tag{15}$$

This correlation for $c_f$ is needed to form the nondimensional distance from the wall $y^+$ used in the empirical equation of Reichardt for eddy diffusivity of momentum as follows:

$$\epsilon_M^c/\nu = \frac{\kappa y^+}{6}\left(1 + \frac{y}{y_{cl}}\right)\left[1 + 2\left(\frac{y}{y_{cl}}\right)^2\right] \tag{16}$$

Since the Reichardt correlation is only valid in the turbulent core region of the coolant (i.e., the region away from the channel walls), the Van Driest correlation is used as follows to form an approximation for eddy diffusivity near the walls:

$$\epsilon_M^w/\nu = \left\{\kappa y^+ \left[1 - \exp\left(-y^+/A^+\right)\right]\right\}^2 \frac{\partial u^+}{\partial y^+} \tag{17}$$

The $y$ value at which the two expressions for eddy diffusivity are equal determines the location of the boundary separating the core and wall regions. Equations (16) and (17) are only defined over $0 \le y \le y_{cl}$, and must be extended symmetrically about $y = y_{cl}$.

The eddy diffusivity for heat transfer $\epsilon_H$ is determined by using the following correlation for turbulent Prandtl number given in reference 9:

$$\frac{1}{\text{Pr}_t} = \frac{1}{2\text{Pr}_{t_\infty}} + C\,\text{Pe}_t\sqrt{\frac{1}{\text{Pr}_{t_\infty}}} - (C\,\text{Pe}_t)^2 \times \left[1 - \exp\left(-\frac{1}{C\,\text{Pe}_t\sqrt{\text{Pr}_{t_\infty}}}\right)\right] \tag{18}$$

where the constants $C$ and $\text{Pr}_{t_\infty}$ are given as 0.2 and 0.86, respectively. The variation of $\text{Pr}_t$ in the flow results from the dependence of $\text{Pe}_t$ on $\epsilon_M$. The value for $\epsilon_H$ is then found from the following simple relation:

$$\epsilon_H = \epsilon_M/\text{Pr}_t \tag{19}$$

### Numerical Models

The algorithms that are used to solve the preceding equations are summarized in this section. The finite-difference methods used to calculate the velocity profiles for developing laminar flow and for turbulent flow of the coolant in the channel are given first. The algorithm for the time-dependent solution for temperatures in the coupled coolant-skin system is then presented. Although a new computer code was written for the present study, the numerical methods incorporated in it are standard.

***Laminar velocity calculation.*** The velocity field for laminar flow in the channel is governed by equations (1) to (5), with $\epsilon_M$ equal to zero. These equations are parabolic in the $x$ direction, so the solution for $u$ and $v$ can be found by marching downstream and solving for the velocities at each consecutive $x$ station by using the method described in reference 10. The details of the method are given in the reference, so only a brief description follows. The channel region is discretized into a rectangular array of nodes, and the finite-difference analog of equation (1) is formed. The velocities $u$ and $v$, which multiply $\partial u/\partial x$ and $\partial u/\partial y$, respectively, make the equation nonlinear; therefore, these velocities are "lagged" (i.e., set to be their values at the previous $x$ station) to linearize the problem. The finite-difference scheme is central, except for the derivative $\partial u/\partial x$, which is "upwinded" (i.e., taken to be a one-sided difference scheme biased in the upstream direction) to enhance stability. The values of $u$ at each $x$ station are calculated by solving a tridiagonal system of equations. The pressure-gradient term is unknown, so a secant iteration is used to determine the value of $dp/dx$ that satisfies an integrated form of continuity as given by

$$\bar{u} = \frac{1}{y_{cl}}\int_0^{y_{cl}} u\,dy \tag{20}$$

Because the finite-difference analog of equation (1) has been linearized, velocity solutions for only two estimates of $dp/dx$ are needed to determine the correct value of $dp/dx$. However, since $dp/dx$ for a developing flow is not constant, this procedure must be repeated at every $x$ station. After the values for $u$ have been determined at a given $x$ station, the values for $v$ are determined by

a simple trapezoidal integration of the finite-difference analog of equation (2).

***Turbulent velocity calculation.*** For fully developed flow in the channel, the left-hand side of equation (1) is zero, and the pressure gradient is constant. The first integral of the resulting equation is then

$$[\nu + \epsilon_M(y)]\frac{du}{dy} = \frac{1}{\rho}\frac{dp}{dx}(y - y_{cl}) \tag{21}$$

where the boundary condition given in equation (4) has been applied. A numerical integration of $du/dy$ in equation (21) with the boundary condition of equation (3) at $y = 0$ gives the $u$-velocity profile; however, the pressure gradient is a free parameter that must be adjusted to satisfy the continuity equation as given by equation (20). The correct value of $dp/dx$ is found by using a bisection technique. An interval of $dp/dx$ values is formed that contains the correct value of $dp/dx$. Since $dp/dx$ is less than zero, this interval has zero as the upper boundary, and a large negative value is assumed for the lower boundary. The midpoint, which divides this interval into two subintervals, is determined, and equations (20) and (21) are solved by using $dp/dx$ values from the midpoint and both boundaries of the interval. The resulting values of $\bar{u}$ are compared with the input value; the subinterval with values of $\bar{u}$ that bound the correct value is retained. The process is repeated until the calculated values of $\bar{u}$ agree with the input value to within a relative error of 0.1 percent. A trapezoidal integration formula is used for all the integrals.

***Temperature calculation.*** The temperatures in the coolant and the skin are determined by integrating the time-dependent energy equations (eqs. (6) and (7)) to steady state. Solving the steady-state problem by using transient equations is a computationally efficient iterative technique for the large number of unknown temperatures (over 2 500 000 for some cases). This method is made stable by an appropriate choice of the time step. The velocities (and $\epsilon_H$ when the flow is turbulent) are known from the previous calculations, so these equations are linear equations for temperature. The second-order-accurate, three-point, time-differencing formula of Beam and Warming (ref. 11) is used to advance the solution in time as follows:

$$\Delta T^n = \frac{2\Delta t}{3}\frac{\partial \Delta T^n}{\partial t} + \frac{2\Delta t}{3}\frac{\partial T^n}{\partial t} + \frac{1}{3}\Delta T^{n-1} \tag{22}$$

where $T^n = T(t = t^n)$ and $\Delta T^n = T^{n+1} - T^n$. In this equation, data at time levels $n$ and $n - 1$ are assumed to be known, and the temperatures at time level $n + 1$, which is implicit in $\Delta T^n$, are to be determined. Substitutions for the time derivatives in equation (22) are made by using equation (6) in the coolant region and equation (7) in the skin region. The resulting equations for $\Delta T^n$ contain only spatial derivatives. To form a system of discrete equations for $\Delta T^n$, the skin region is discretized into a rectangular array of nodes that is appended to the array of nodes previously defined for calculating velocities of the coolant region. The spatial temperature derivatives are replaced with their finite-difference analogs on these nodes. The resulting system of equations for the nodal temperatures is approximately factored as in reference 11. A similiar procedure is used for interface nodes $(x^i, y_i^j)$ between the coolant and skin, but the following energy balance equation is used in place of equations (6) and (7):

$$\frac{\partial T^n(x^i, y_i^j)}{\partial t} = \frac{q_y^- - q_y^+ + q_x^- - q_x^+}{\Delta x(k_c\Delta y_c/2\alpha_c + k_s\Delta y_s/2\alpha_s)} \tag{23}$$

with

$$q_x^- = -(k_c\Delta y_c/2 + k_s\Delta y_s/2) \times [T^n(x^i, y_i^j) - T^n(x^{i-1}, y_i^j)]/\Delta x \tag{24}$$

$$q_x^+ = -(k_c\Delta y_c/2 + k_s\Delta y_s/2) \times [T^n(x^{i+1}, y_i^j) - T^n(x^i, y_i^j)]/\Delta x \tag{25}$$

$$q_y^- = \frac{-k_s\Delta x}{\Delta y_s}[T^n(x^i, y_i^j) - T^n(x^i, y_i^{j-1})] \tag{26}$$

$$q_y^+ = \frac{-k_c\Delta x}{\Delta y_c}[T^n(x^i, y_i^{j+1}) - T^n(x^i, y_i^j)] \tag{27}$$

Because of the approximate factorization, only tridiagonal matrix systems of equations need be solved at each time step. The algorithm has been found to be very reliable and efficient in this application.

## Verification Cases

The models for both laminar- and turbulent-flow conditions are compared with published results to demonstrate their correctness. The basis for comparison is the nondimensionalized heat transfer from the skin to the coolant—the Nusselt number. The Nusselt number is determined as follows:

$$\mathrm{Nu} = \frac{\dot{q}_i D_h}{k_c(T_i - T_b)} = \left|\frac{\partial T_c}{\partial y}\right|_i \frac{D_h}{T_i - T_b} \tag{28}$$

where the bulk temperature is given by

$$T_b = \frac{1}{\bar{u}h_c}\int_0^{h_c} Tu\,dy \tag{29}$$

***Laminar cases.*** The correctness of the numerical model for laminar coolant flow is demonstrated by comparisons with the computational results published in reference 12 for the simultaneous growth of laminar hydrodynamic and thermal boundary layers. The heat input in the reference is a uniform heat flux at the coolant boundary. In the present model, however, the heat-flux condition is imposed on the outer surface of the skin. The desired uniform-heat-flux boundary condition at the coolant-skin interface is approximated to within 0.5 percent in the present model by using a uniform heat flux on the outer surface of the skin, a skin thickness 1 percent of the channel height (i.e., $h_s = 0.01h_c$), and a skin thermal conductivity equal to the coolant thermal conductivity.

The Nusselt number calculated by using the present code is compared in figure 5 with the results of reference 12 for a wide range of Prandtl numbers and nondimensional lengths $x^+$. For the results shown, the number of equally spaced nodes positioned in the model across the channel height $h_c$ and skin thickness $h_s$ is 340 nodes and 16 nodes, respectively. The streamwise direction is discretized with 2400 equally spaced nodes over $0 \leq x^+ \leq x^+_{\max}$, where $x^+_{\max} = 0.12$. The determination of convergence with mesh refinements was made by recomputing the solution with $x^+_{\max} = 0.006$ (which doubles the number of nodes per inch in the $x$ direction) and by doubling the number of nodes in the $y$ direction. No appreciable differences were found between corresponding solutions of the coarse- and fine-spaced models, which indicates that the results shown in the figure are independent of mesh.

As can be seen in figure 5, there is very good agreement between the published and present results; the difference between the two is less than 10 percent for all values of $x^+$ and at all Prandtl numbers. The agreement is better for higher values of $x^+$ and for higher Prandtl numbers. The Nusselt number results can be extrapolated to infinity as $x^+$ approaches zero, because $T_i - T_b$ in the denominator of equation (28) also goes to zero. A detailed investigation of the differences between the published and the present results has not been conducted. However, the differences may be explained, in part, by the differences in the two solution procedures.

***Turbulent cases.*** The correctness of the numerical model for turbulent coolant flow is demonstrated by comparisons with the numerical results of Hatton and Quarmby (ref. 13) for the growth of the thermal boundary layer with a fully developed hydrodynamic boundary layer. As in the laminar verification cases, the thermal boundary condition of the reference is a uniform heat flux at a coolant boundary instead of at the outer face of a skin; so the assumptions used in the

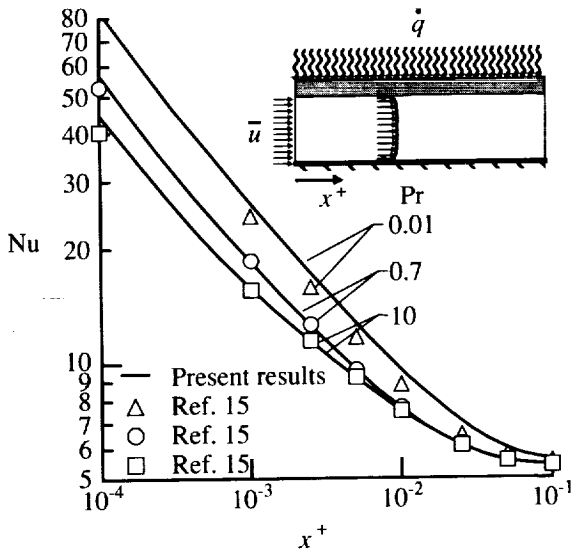


Figure 5. Comparison of published and calculated laminar Nusselt numbers.

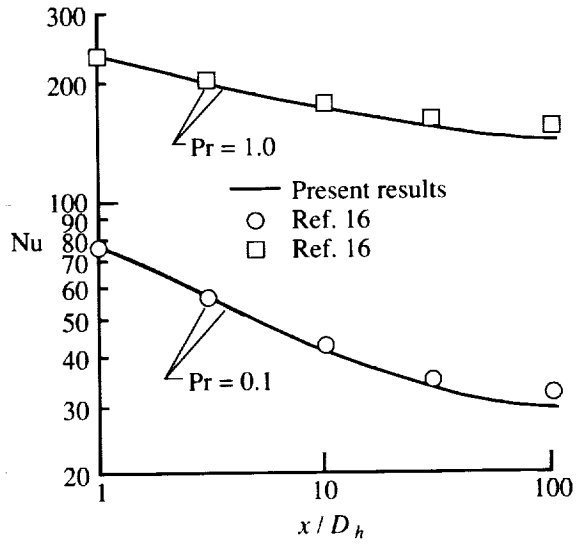


Figure 6. Comparison of published and calculated turbulent Nusselt numbers for $R = 7.36 \times 10^4$.

laminar verification cases for the geometry and properties of the skin are utilized. In the present calculations, $\mathrm{Pr}_t = 1.0$ was used to agree with the value used in the reference. Calculated Nusselt numbers are compared with the reference results in figure 6 for Pr = 0.1 and 1.0 at $R = 7.36 \times 10^4$ for $1 \leq x/D_h \leq 100$. There are 1300 and 19 equally spaced nodes positioned in the model across the channel height $h_c$ and skin thickness $h_s$, respectively. The large number of nodes in the coolant region is required to resolve the viscous sublayer. The streamwise coordinate is discretized with

1000 nodes over $0 \leq x/D_h \leq 100$. This streamwise discretization is satisfactory, since a case with 1000 nodes over $0 \leq x/D_h \leq 10$ gives essentially the same results.

There is good agreement between the published and present results at both Prandtl numbers. The agreement is better for lower values of $x/D_h$. Maximum differences of 6 percent and 8 percent are found at $x/D_h = 100$ for Pr = 1.0 and Pr = 0.1, respectively.

## Results

In this section, the results of flow and thermal analyses are presented to gauge the capabilities of tangential convective cooling. The specific problem analyzed is representative of cooling a copper-alloy, engine cowl leading edge subject to shock-shock interaction heating. The measure of the cooling capability is the magnitude of the maximum temperature of the copper-alloy skin. For many of the cases considered, the results indicate that the maximum skin temperature exceeds the 1200°F maximum-use temperature of copper alloys. Also, in many cases the coolant temperature locally exceeds the assumed temperature used to determine the constant coolant properties. Nevertheless, the results indicate the relative cooling effectiveness of the different coolants and flow conditions. Nominal analysis conditions are given for laminar and turbulent flow of three coolants. Detailed thermal results are given for the nominal conditions of one of these coolants. Results are presented that illustrate the effects of variations in coolant mass flow, heated-region extent, skin thickness, and coolant temperature for all three coolants.

### Analysis Conditions

The geometry of the idealized cooling problem is illustrated in figure 4, and the nominal values for the geometry parameters are given in table 1. As shown in the table, the values of the geometry parameters $l$ and $x_{\max}$ are determined based on whether laminar or turbulent coolant flow is considered. In the laminar cases, the velocity boundary layer develops from a uniform velocity profile at the inlet. A characteristic length from the location of a shock-shock interaction heating zone to a coolant inlet manifold for a cowl leading edge is on the order of an inch, but may be as large as 6 in. because of space constraints in the leading edge. Thus, the model for laminar-flow cases utilizes values of $l = 1$ in. and $x_{\max} = 2$ in. In turbulent-flow cases, the hydrodynamic flow is fully developed, so the values used for these streamwise lengths are less important. The only requirement is that the streamwise boundary conditions given by equations (13) and (14) be far enough from the heated zone to have no effect on the maximum calculated temperature. Values of $l$ and $x_{\max}$ of 0.5 in. and 1.0 in., respectively, were found to be satisfactory.

Table 1. Nominal Geometry Parameters

| Parameter | Laminar flow, in. | Turbulent flow, in. |
|---|---|---|
| $h_c$ | 0.030 | 0.030 |
| $h_s$ | .020 | .020 |
| $w$ | .015 | .015 |
| $l$ | 1.000 | .500 |
| $x_{\max}$ | 2.000 | 1.000 |

Table 2. Nominal Thermal and Flow Conditions

| Coolant | $T_b'$, °F | $T_{\text{in}}$, °F | $\bar{u}$, $\frac{\text{ft}}{\text{sec}}$ |
|---|---|---|---|
| Hydrogen | −60 | −360 | 600 |
| Water | 350 | 65 | 200 |
| Sodium | 400 | 250 | 200 |

The nominal thermal and flow conditions for the three coolants are given in table 2. The temperature at which the thermodynamic and transport properties of the coolants are evaluated is $T_b'$. In the present study, these properties are assumed to be constant with nominal values corresponding to the temperatures $T_b'$ given in table 2. The actual temperatures are obtained by adding the inlet temperature $T_{\text{in}}$ given in table 2 to the temperature rise that is computed by the numerical models. The nominal average coolant velocity $\bar{u}$ given in the table is also the inlet coolant velocity for the laminar coolant flow cases.

Coolant properties for supercritical, cryogenic hydrogen, liquid water, and liquid sodium are given in tables 3, 4, and 5, respectively; the entries marked with an asterisk (*) indicate the value of $T$ used as $T_b'$ of the nominal analysis conditions. The properties for hydrogen and water are obtained from the computer program of references 14 and 15, and the properties for sodium are found from the computer program of reference 16, except for specific heat, which is taken from reference 17. As seen from these tables, the Prandtl numbers of these coolants cover a wide range and are representative of different classes of coolants.

The copper-alloy skin has a conductivity $k_s$ of 0.0556 Btu/ft-sec-°F. Since only the steady-state response is desired, the skin thermal diffusivity $\alpha_s$ and the time step $\Delta t$ are free parameters that can be adjusted to accelerate convergence to a steady state. In

Table 3. Hydrogen Properties

[$p$ = 2500 psi]

| $T$, °F | $\rho$, $\frac{\text{lbm}}{\text{ft}^3}$ | $c_p$, $\frac{\text{Btu}}{\text{lbm-°F}}$ | $k$, $\frac{\text{Btu}}{\text{ft-sec-°F}}$ | $\mu$, $\frac{\text{lbm}}{\text{ft-sec}}$ | Pr |
|---|---|---|---|---|---|
| −360 | 3.734 | 3.147 | $2.057 \times 10^{-5}$ | $5.559 \times 10^{-6}$ | 0.851 |
| −260 | 2.005 | 4.024 | $2.308 \times 10^{-5}$ | $4.126 \times 10^{-6}$ | .720 |
| −60* | 1.038 | 3.912 | $3.233 \times 10^{-5}$ | $5.329 \times 10^{-6}$ | .645 |
| 340 | .546 | 3.507 | $4.427 \times 10^{-5}$ | $8.038 \times 10^{-6}$ | .637 |

Table 4. Water Properties

[$p$ = 750 psi]

| $T$, °F | $\rho$, $\frac{\text{lbm}}{\text{ft}^3}$ | $c_p$, $\frac{\text{Btu}}{\text{lbm-°F}}$ | $k$, $\frac{\text{Btu}}{\text{ft-sec-°F}}$ | $\mu$, $\frac{\text{lbm}}{\text{ft-sec}}$ | Pr |
|---|---|---|---|---|---|
| 65 | 62.48 | 0.997 | $9.637 \times 10^{-5}$ | $6.976 \times 10^{-4}$ | 7.215 |
| 150 | 61.32 | .997 | $1.058 \times 10^{-4}$ | $2.892 \times 10^{-4}$ | 2.725 |
| 350* | 55.76 | 1.046 | $1.091 \times 10^{-4}$ | $1.030 \times 10^{-4}$ | .987 |
| 500 | 48.96 | 1.185 | $9.742 \times 10^{-5}$ | $6.825 \times 10^{-5}$ | .830 |

Table 5. Sodium Properties

| $T$, °F | $\rho$, $\frac{\text{lbm}}{\text{ft}^3}$ | $c_p$, $\frac{\text{Btu}}{\text{lbm-°F}}$ | $k$, $\frac{\text{Btu}}{\text{ft-sec-°F}}$ | $\mu$, $\frac{\text{lbm}}{\text{ft-sec}}$ | Pr |
|---|---|---|---|---|---|
| 250 | 57.68 | 0.328 | $1.398 \times 10^{-2}$ | $4.148 \times 10^{-4}$ | 0.0097 |
| 400* | 56.51 | .320 | $1.327 \times 10^{-2}$ | $3.076 \times 10^{-4}$ | .0074 |
| 550 | 55.30 | .313 | $1.258 \times 10^{-2}$ | $2.402 \times 10^{-4}$ | .0060 |
| 700 | 54.09 | .307 | $1.191 \times 10^{-2}$ | $1.982 \times 10^{-4}$ | .0051 |

all cases, the magnitude of the heat flux, $\dot{q} = \dot{Q}$, is 50 000 Btu/ft$^2$-sec.

The "fineness" of the discretization (i.e., the mesh size) for the channel and the skin is very important for accurate results. As the discretization becomes finer, the results become independent of mesh, but an excessively fine discretization becomes computationally expensive. For laminar coolant flow, an acceptable discretization of the channel and the skin was obtained by using 300 nodes across the height of the channel, 20 nodes across the thickness of the skin, and 1000 nodes per inch in the streamwise direction. The need for this level of resolution was determined from a convergence study in which the number of nodes was doubled until the calculated maximum skin temperature changed by less than 1 percent between cases. For the turbulent coolant flow cases, it was necessary to increase the number of nodes across the height of the channel to 600 for sodium coolant and to 2500 for hydrogen and water coolants to compute the maximum skin temperature within the convergence criterion.

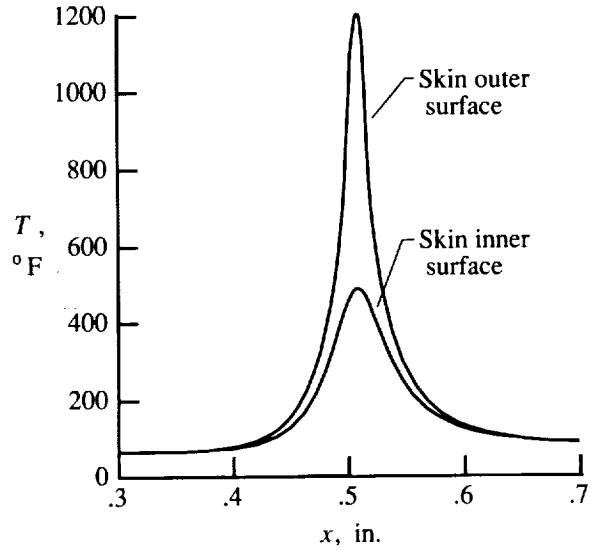


Figure 7. Temperatures along outer and inner faces of heated skin for nominal conditions and turbulent-flow, water-cooled skin.

## Detailed Thermal Results

In this section, some detailed results are given for the nominal case of a turbulent-flow, water-cooled skin. These details are useful because they show the structure of the temperature field in the vicinity of the localized thermal load, improve understanding of the maximum skin-temperature results, and suggest simplifications that allow a correlation of the parametric results, which are discussed in the appendix.

The temperatures on both the outer (heated) and inner (cooled) surfaces of the skin are shown in figure 7. Because the water coolant is very effective for this case, there is essentially no influence on the temperature 0.1 in. upstream of the thermal load, which starts at $x = 0.5$ in. and ends at $x = 0.515$ in., and there is only a small residual effect downstream of the load. However, the outer-surface temperature rises rapidly in the vicinity of the thermal load to a maximum of 1206°F. The inner-surface temperature has a maximum of 489°F at about the same streamwise location; this creates a temperature difference of over 700°F through the thickness of the skin. The extreme thermal stresses that would accompany such a large temperature difference are important but are not evaluated in the present study.

Another view of the temperature increases caused by the localized thermal load is given in figure 8. In

this figure, even though the $y$-axis is expanded by a factor of four, the two-dimensional nature of the temperature contours near the localized thermal load, beginning at $x = 0.50$ in., is apparent. A large temperature difference across the skin occurs near the location of the thermal load; however, slightly upstream and downstream of this location, there is essentially no temperature difference across the skin. The contours that nearly align with the $y$-axis indicate that the skin is behaving as a one-dimensional fin away from the location of the localized thermal load. The temperature contours are closely spaced in the coolant region near the coolant-skin interface because of the low effective conductivity in the viscous sublayer and the convection of the coolant. Although the coolant temperature approaches 500°F locally, the bulk of the coolant is at a relatively low temperature.

The Nusselt number and heat flux at the coolant-skin interface are shown in figure 9. Most of the heat enters the coolant in the narrow region that surrounds the localized thermal load. In this case, the maximum heat flux entering the coolant is less than 12 000 Btu/ft$^2$-sec, while the applied heat flux is 50 000 Btu/ft$^2$-sec. Thus, a considerable spreading of the input heating by the skin occurs. The Nusselt number behaves in a relatively simple manner near the localized thermal load. Upstream of the load, the Nusselt number is a high "plateau" value, and it rapidly decreases in the region of the thermal load to a low "floor" value downstream of the thermal load.

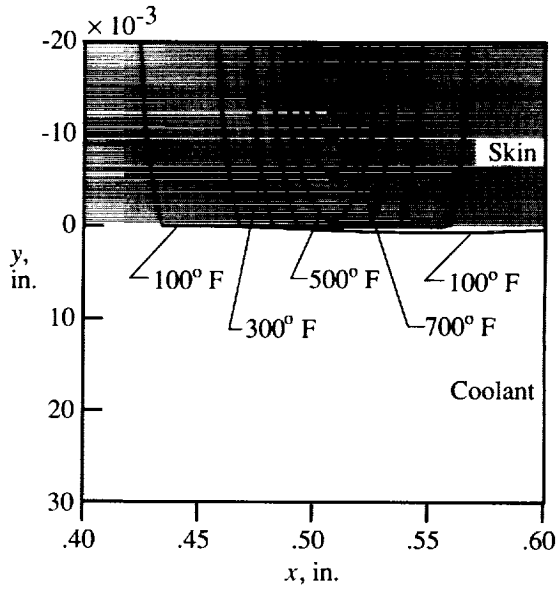


Figure 8. Temperature contours in skin and coolant near localized thermal load. ($y$-axis expanded 4×.)

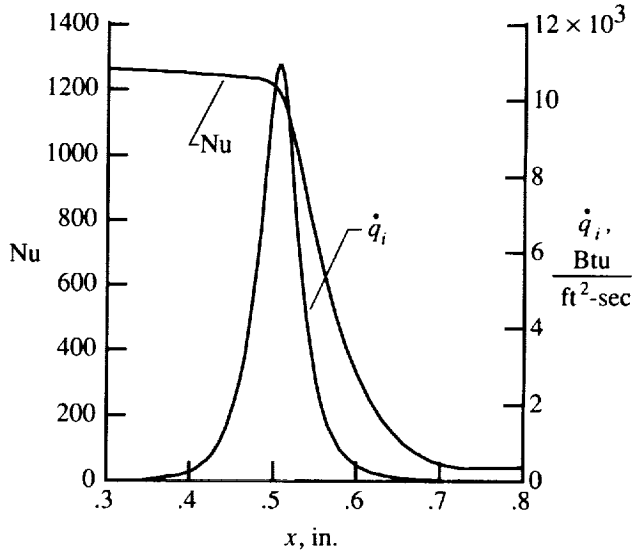


Figure 9. Nusselt number and heat flux entering coolant at coolant-skin interface for nominal conditions with turbulent water coolant flow.

### Coolant Velocity Effects

The variation of maximum skin temperature with velocity for the laminar flow of the three coolants is given in figure 10. The other parameters are assumed to be the nominal values. The maximum skin temperature for a laminar hydrogen coolant flow is very sensitive to the average coolant velocity with a temperature above 6000°F at 100 ft/sec and a temperature slightly below 3500°F at 800 ft/sec. From these extremely high temperatures, a laminar flow of hydrogen will not be effective in cooling the leading edge. The maximum skin temperature is shown for a laminar water coolant flow with velocities from 50 to 250 ft/sec. The temperature at 50 ft/sec is slightly below 2900°F, and it drops to slightly more than 2000°F at 250 ft/sec. The laminar flow of water appears to be much more effective than that of hydrogen in this cooling application; however, it is important to remember that the mass-flow rate of water is much higher than that of hydrogen for the same velocity because of the large difference in density of the two coolants. A system-level study is needed to determine if the indicated velocities for water coolants and hydrogen coolants are reasonable for the specific application. The maximum skin-temperature variation for a laminar sodium coolant flow is also shown in figure 10. This coolant appears to be the only one for which acceptable temperatures can be achieved when laminar flow is assumed. The temperature at 50 ft/sec is slightly below 1300°F, and at 250 ft/sec it is about 1175°F. The density of sodium is comparable to water, so the improvement in cooling effectiveness can be attributed to the high thermal conductivity of the

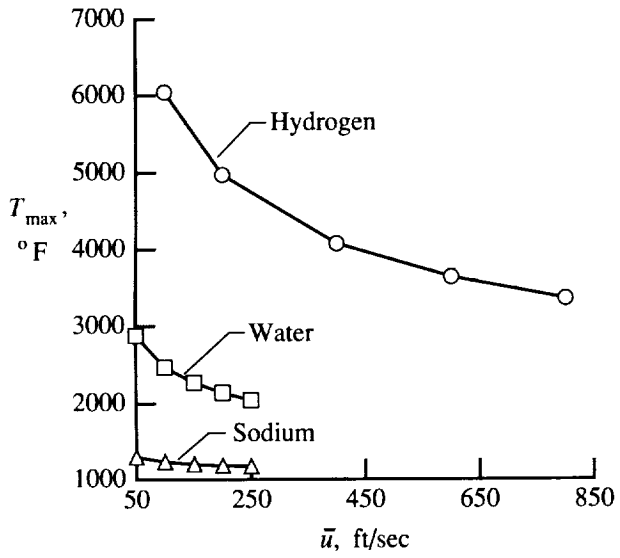


Figure 10. Maximum skin-temperature variation with coolant velocity for laminar flows of hydrogen, water, and sodium coolants at nominal conditions.

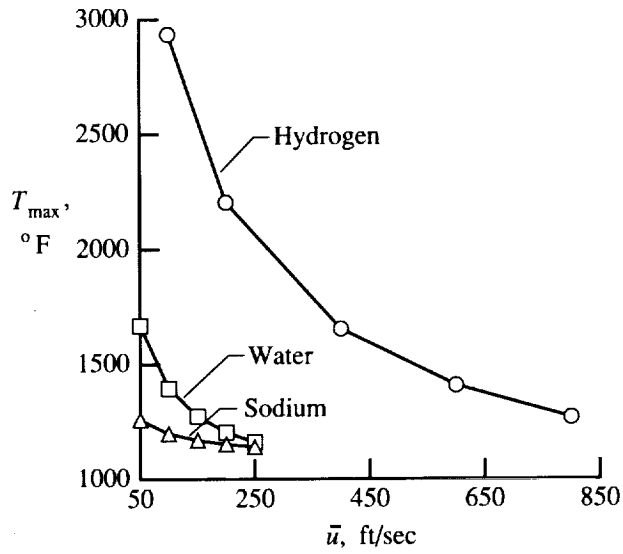


Figure 11. Maximum skin-temperature variation with coolant velocity for turbulent flows of hydrogen, water, and sodium coolants at nominal conditions.

sodium coolant. Again, a system-level study is needed to determine if the indicated flow rates are reasonable for the application.

The situation changes dramatically when the coolant flow is assumed to be turbulent. The variation of maximum skin temperature with coolant velocity for turbulent flows of hydrogen, water, and sodium is shown in figure 11. The results shown in this figure should be compared with those of figure 10, in which the coolant is laminar. Notice that the temperature scale of figure 11 is expanded over two times that of figure 10. The maximum temperatures for turbulent hydrogen coolant flow are less than half the corresponding values for laminar hydrogen flow. The maximum skin temperature at a coolant velocity of 800 ft/sec is now only 1270°F, which is nearly down to the temperature limit of the copper-alloy skin; the maximum skin temperature was 3500°F for laminar flow. If the increased cooling effectiveness due to surface roughness and coolant passage curvature (such as in ref. 18) is considered, it appears possible that hydrogen coolant may be used with a copper leading edge. The maximum skin temperatures that result from turbulent flows of water and sodium coolants are also shown in figure 11. At a velocity of 50 ft/sec, the maximum skin temperature for a turbulent flow of water is about 1670°F—a reduction of about 1200°F from the laminar result. At 250 ft/sec, the maximum temperature for turbulent water coolant flow is 1160°F—about 900°F lower than the laminar value. There is only about a 30°F temperature difference between the turbulent results for sodium in figure 11 and the laminar results in figure 10. This small difference is believed to be a result of the dominance of molecular thermal diffusivity for the highly conductive sodium. There is very little difference between the results for turbulent flow of the water and sodium coolants as the velocities approach 250 ft/sec. However, the temperature of the water entering the leading edge is almost 200°F lower than that of the sodium coolant. Thus, it appears that liquid metals offer no advantage over water for the higher coolant velocities when the flow can be assured to be turbulent, since both coolants are capable of cooling the skin below the temperature limit of copper alloys. In summary, from the study of coolant velocity effects, a liquid-sodium-cooled engine cowl leading edge appears viable from a maximum-temperature standpoint for both laminar and turbulent coolant flows, and a leading edge cooled with water or hydrogen can only be viable if the coolant flow is made turbulent.

### Effects of Heated-Region Extent

The sensitivity of maximum temperature to the extent of the heated region is important, because the influence of lateral conduction in the skin diminishes and the maximum skin temperature rises as the length of this region increases. Also, although the nominal value of $w = 0.015$ in. chosen for the extent of the thermal load in the present study is based on the experimental results in reference 2, there is uncertainty in the extent of the region of intense heating due to the shock-shock interaction. For these reasons, the effect of the extent of the heated region on maximum skin temperature is important, and a cooled leading edge with a low sensitivity of maximum skin temperature to variations in $w$ is desired.

The effect of variations in $w$ on maximum temperature in the skin is shown for laminar coolant flow in figure 12, and for turbulent coolant flow in figure 13. The temperature differences as a function of $w$ in these figures are the changes in maximum skin temperature from the value calculated by using the nominal analysis conditions (i.e., $\Delta T_s = T_{s,\max} - T_{s,\max,\text{nom}}$) shown in tables 1 and 2. A positive $\Delta T_s$, which indicates that the cooling is less effective than the nominal conditions, is undesirable. The temperature variations for all the coolants are nearly linear over the range of $w$ investigated. The laminar-flow results in figure 12 are the most sensitive to variations in $w$ with slopes of 240 000°F/in., 111 000°F/in., and 36 000°F/in. for hydrogen, water, and sodium, respectively. For the nominal conditions described previously, the skin temperatures for laminar hydrogen and water coolant flows are significantly higher than the 1200°F limit of copper alloys. However, the nominal laminar sodium coolant flow gives feasible temperatures, and this coolant is also the least sensitive (i.e., has the smallest slope) to variations in extent of the heated region.

For turbulent flow, all three coolants yield temperatures near or below the skin-temperature limit. Since the same scale is used for the turbulent results of figure 13 as for the laminar results of figure 12, it is evident that the slopes of the temperature variations for turbulent flows are less than the corresponding slopes for laminar flow. The turbulent coolant flow results in figure 13 have slopes of 91 000°F/in., 49 000°F/in., and 34 000°F/in. for hydrogen, water, and sodium, respectively. Thus, in changing the assumed flow condition from laminar to turbulent, the hydrogen-cooled skin shows the greatest decrease in sensitivity to changes in $w$, the water-cooled skin shows a percentage decrease slightly smaller than the hydrogen, and the sodium coolant has about the same sensitivity. The latter result for sodium reinforces the previous finding that only minor improvements are obtained by including turbulent diffusivity for liquid-metal coolants.

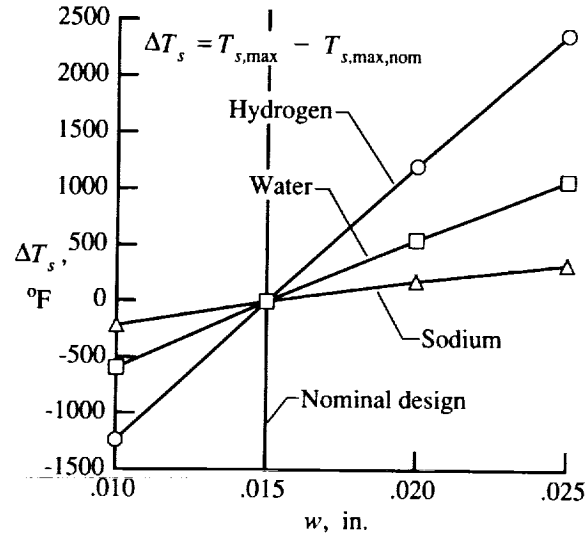


Figure 12. Maximum skin-temperature variation from nominal condition with heated-region extent for laminar coolant flow.

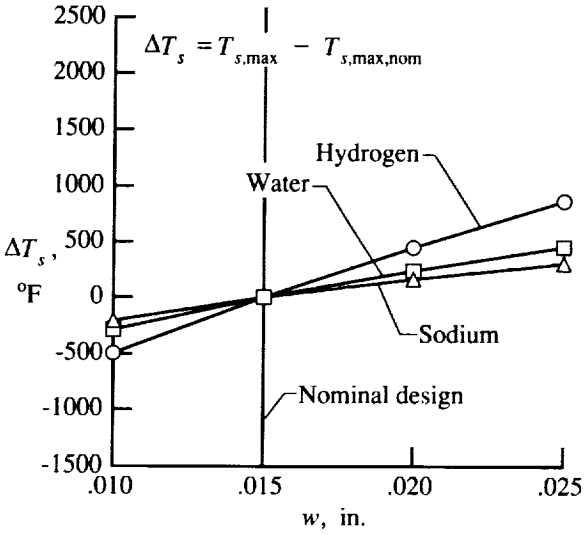


Figure 13. Maximum skin-temperature variation from nominal condition with heated-region extent for turbulent coolant flow.

## Effects of Skin Thickness

The effects of variations in skin thickness on maximum skin temperature for laminar coolant flow are shown in figure 14. As in the preceding section, the temperature variations shown are the changes in maximum skin temperature from the values calculated by using the nominal analysis conditions in tables 1 and 2. Hydrogen is the most sensitive to variation in skin thickness, with an average slope of −75 000°F/in., followed by water, with an average slope of −21 000°F/in., and then sodium, with a slope of 16 000°F/in. Of the three coolants, only sodium shows a near-linear temperature variation.

The sensitivities of the maximum skin temperature to changes in skin thickness for turbulent coolant flow are plotted in figure 15, and the same scale is used as in figure 14. The temperature variation of the turbulent-flow, sodium-cooled skin shows little change from that of laminar flow in figure 14; however, the magnitude of the temperature variation for a hydrogen-cooled skin is significantly reduced. The temperature variation for a water-cooled skin is lower in magnitude than the laminar-flow cases in figure 14, but the slope

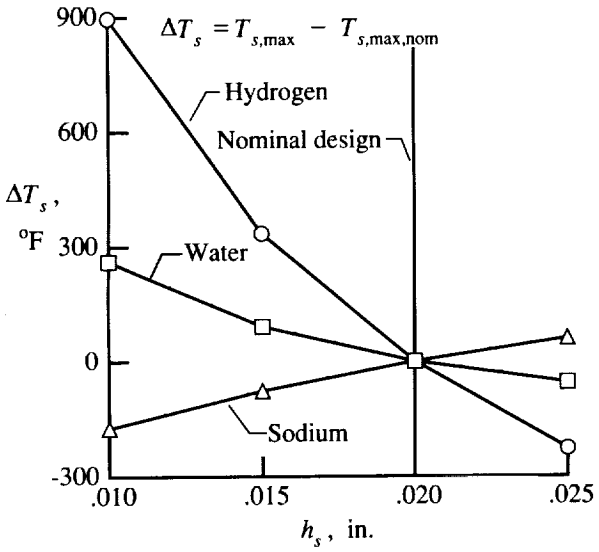


Figure 14. Maximum skin-temperature variation from nominal condition with skin thickness for laminar coolant flow.

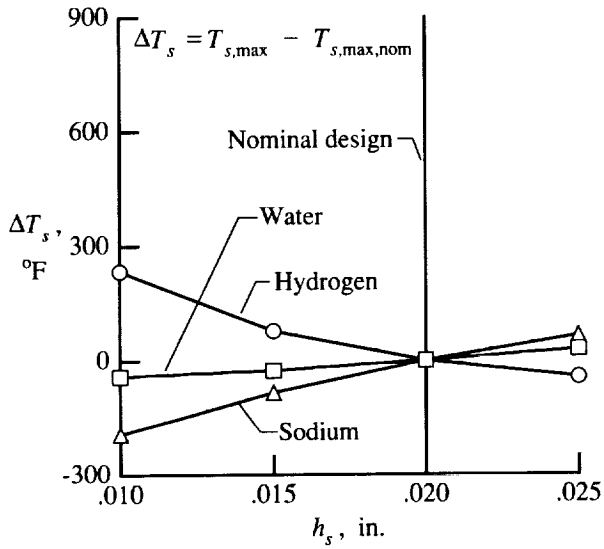


Figure 15. Maximum skin-temperature variation from nominal condition with skin thickness for turbulent coolant flow.

of the variation is opposite in sign. If the conduction through the thickness of the skin is considered as one dimensional, a decrease in skin thickness is expected to result in a decrease in maximum temperature; thus, the results with negative slopes in figures 14 and 15 must result from lateral conduction effects.

To better understand the negative slopes in figures 14 and 15, the set of cases studied for a laminar-flow, water-cooled skin was expanded to include skin thicknesses as large as 0.25 in. The maximum skin temperature and the coolant-skin interface temperature at the maximum skin-temperature location for these cases are shown in figure 16. The temperatures presented in the figure have been reduced by the inlet temperature to show temperature rise from the channel inlet. Also shown in the figure is the heat flux entering the coolant at the same $x$ location as the maximum temperature. As was observed in figure 14, the skin temperature decreases with increasing skin thickness at the smaller values of $h_s$. However, the maximum skin temperature passes through a minimum near $h_s = 0.065$ in. and then increases with increasing skin thickness. A minimum in $T_{max}$ as a function of skin thickness has also been found for the sodium-cooled skin at very small skin thicknesses; it is believed that the other curves in figures 14 and 15 would also have minima if the analysis ranges were suitably extended. The questions as to why a minimum exists and why the maximum skin temperature increases with decreasing skin thickness at the smaller skin thickness values can be answered by using the curves in figure 16.

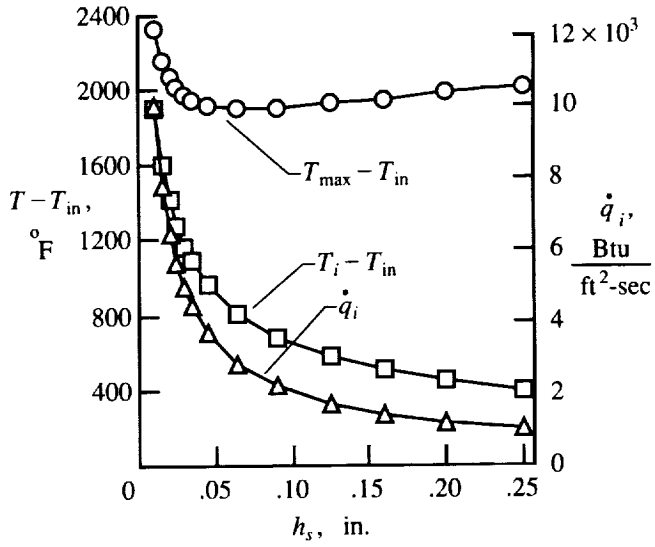


Figure 16. Variations of outer-face skin temperature, coolant-skin interface temperature, and coolant-skin interface heat flux with skin thickness at the $x$ location of maximum skin temperature for laminar water coolant flow.

The temperature difference across the thickness of the skin, given by the distance between the two temperature curves in figure 16, always decreases with decreasing skin thickness. This result conforms with the intuitive expectation that decreasing skin thickness should correspond to a decreasing temperature difference. However, the maximum skin temperature depends on both the temperature difference across the thickness of the skin and the temperature difference across the coolant "film." The temperature difference across the film is given by $T_i - T_b$, where $T_b$ is given by

equation (29). Since $T_b \approx T_{in}$, the temperature difference is also well represented by the curve for $T_i - T_{in}$ in figure 16. Thus, as skin thickness is decreased, a minimum temperature occurs when the increases in the temperature difference across the film become larger than the decreases in the temperature difference across the skin. This phenomenon is shown in figure 16.

An additional question is, why does the temperature difference across the coolant film increase so rapidly as the skin thickness is decreased? Since $\dot{q}_i = h_H(T_i - T_b) \approx h_H(T_i - T_{in})$, and since $h_H$ has only a small variation with skin thickness, the temperature difference across the coolant film ($\approx T_i - T_{in}$) closely follows the interface heat flux, as shown in figure 16. The interface heat flux and the temperature difference across the coolant film rapidly increase as the skin thickness decreases, because the ability of the skin to distribute the heat by lateral conduction is reduced. The correctness of this explanation is further confirmed in figure 17, which shows that the heat flux at the coolant-skin interface becomes localized and has larger maximum values for thinner skins. Thus, the phenomenon of a minimum in $T_{max}$ with variations of skin thickness ultimately results from two effects the lateral flow of heat in the vicinity of the localized thermal load and the existence of a temperature difference across the coolant film. If the heat flow were one dimensional through the skin thickness, or if a constant-temperature boundary condition were used at the coolant-skin interface, the variation in the maximum skin temperature due to changes in skin thickness would not have a minimum.

### Effects of Coolant Bulk Properties

Since the present analysis utilizes constant properties for the coolant, an investigation of the changes in the maximum skin temperature with variations in the assumed coolant properties was performed. The method of the investigation was to recompute the maximum skin temperatures for the nominal channel geometry by using each of the temperatures shown in tables 3, 4, and 5 as the temperature at which bulk properties are evaluated $T_b'$ . In these calculations, the velocity of the coolant entering the channel was adjusted to keep the same total coolant mass-flow rate as in each of the nominal cases. The inlet temperatures $T_{in}$ of each of the coolants were also kept at their nominal values. The results from this study are no substitute for determining the effects of spatially varying, temperature-dependent coolant properties, but they do establish the sensitivity of the results to gross changes in the coolant properties.

The variations in maximum skin temperature with changes in assumed $T_b'$ for hydrogen, water, and sodium are shown in figures 18, 19, and 20, respectively. These skin-temperature variations $\Delta T_s$ are the changes in

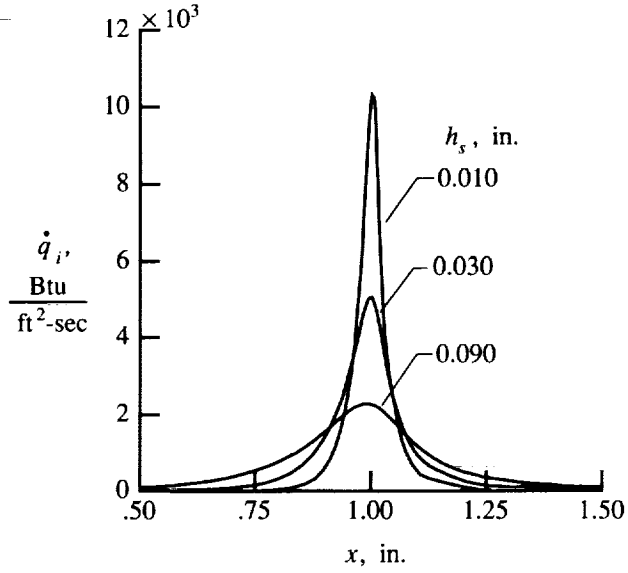


Figure 17. Variation of heat flux at coolant-skin interface with streamwise location for laminar water coolant flow.

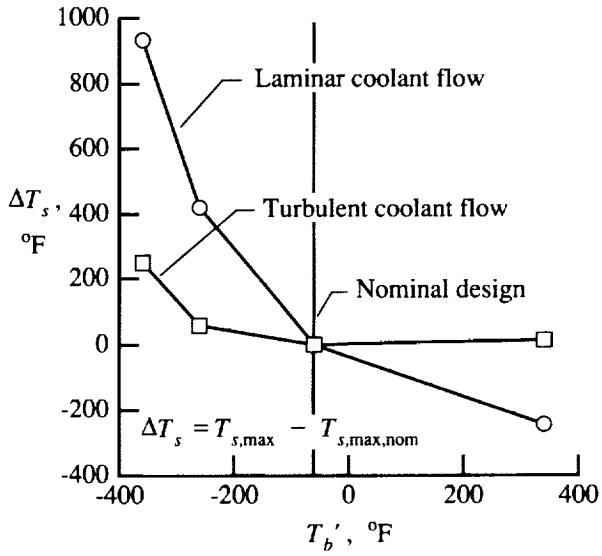


Figure 18. Maximum skin-temperature variation with temperature at which bulk properties are evaluated for laminar and turbulent flows of hydrogen coolant ($\rho\bar{u}$ = 623 lbm/ft$^2$-sec).

maximum skin temperature from the values calculated by using properties at the nominal (asterisked) $T_b'$ values shown in tables 3, 4, and 5 (i.e., $\Delta T_s = T_{s,max} - T_{s,max,nom}$). In figure 18, the variations in maximum skin temperature for laminar flows of hydrogen coolant are about the same order of magnitude as the $T_b'$ variations, and the maximum skin temperature and the

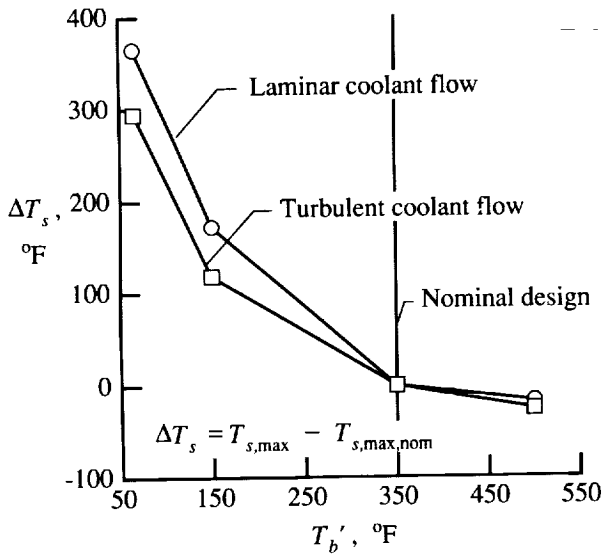


Figure 19. Maximum skin-temperature variation with temperature at which bulk properties are evaluated for laminar and turbulent flows of water coolant ($\rho\bar{u}$ = 11 200 lbm/ft$^2$-sec).

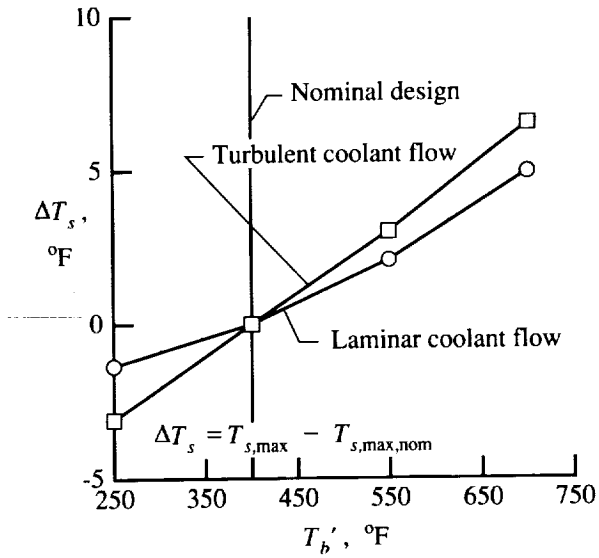


Figure 20. Maximum skin-temperature variation with temperature at which bulk properties are evaluated for laminar and turbulent flows of sodium coolant ($\rho\bar{u}$ = 11 300 lbm/ft$^2$-sec).

sensitivity to the bulk-temperature variations decrease with increasing $T_b'$ over the range indicated. The variation for turbulent flow of hydrogen coolant is much smaller with very little decrease in maximum skin temperature between $T_b' = -260°F$ and $-60°F$; the maximum skin temperature slowly increases above $-60°F$. The maximum skin-temperature variation for both laminar and turbulent flows of water coolant in figure 19 is similar to that of laminar hydrogen in figure 18; the maximum skin temperature and the sensitivity to the $T_b'$ variations decrease with increasing $T_b'$ over the range indicated. In figures 18 and 19, the variation in maximum skin temperature is a large percentage of the 1200°F temperature limit of copper. Thus, the temperature used to determine bulk coolant properties is important for both hydrogen and water coolants. The variation in maximum skin temperature with $T_b'$ of sodium is shown in figure 20. Over the 450°F range in $T_b'$ in the figure, the skin temperature varies by less than 10°F; therefore, the $T_b'$ assumed for sodium is not important.

## Concluding Remarks

A numerical study of the convective cooling of locally heated skins has been performed to assess the capability of tangential convective cooling. The governing differential equations, boundary conditions, and turbulence equations are presented, along with the steps used to discretize them into a model capable of analyzing a two-dimensional coolant flow bounded by the heated skin. Uniform coolant and skin properties have been assumed in all the analyses. The model has been verified by demonstrating the agreement of the calculated Nusselt numbers for a uniformly heated skin with published values for developing laminar and fully developed turbulent hydrodynamic flows over a range of Prandtl numbers.

As a study case, a localized thermal load representative of shock-shock interaction heating of an engine cowl leading edge has been assumed. The effects due to model curvature and channel sidewalls have been ignored. Detailed thermal results are given for a turbulent flow of a water coolant at the nominal analysis conditions. The results from a series of studies that show parametric sensitivities of maximum skin temperature are also presented. Both laminar and turbulent flows of hydrogen, water, and sodium coolants in a copper-alloy leading edge are investigated over ranges of coolant velocity, thermal load extent, skin thickness, and assumed bulk coolant properties.

With a 1200°F temperature limit for a copper-alloy, cowl leading edge, it appears that tangential convective cooling is not feasible for laminar flows of hydrogen and water coolants, but is feasible with a sodium coolant for this application. For turbulent flows, all three coolants yield feasible or near-feasible temperatures for some values of coolant velocity in the ranges investigated. Sodium has the additional advantages of being the least sensitive of the three coolants to flow conditions (laminar or turbulent) and to variations in coolant velocity, extent of the heated region, and the assumed temperature for determining bulk coolant properties. With these advantages, liquid metals, such as sodium, should be seriously considered for the cooling of intense, localized thermal loads.

NASA Langley Research Center
Hampton, VA 23665-5225
March 6, 1991

# Appendix

## Correlation of Maximum Skin Temperatures

The present study presents a large set of numerical results that were obtained from variations of the physical parameters of a specific problem—active cooling of an engine cowl leading edge subjected to shock-shock interaction heating. However, it is desirable to find some simple correlations that will give the same approximate results, or will at least correlate the large number of seemingly unrelated results. Because of the spatially dependent coolant and skin interaction, as well as the lateral conduction in the heated skin, it might appear that no simple correlation could exist. However, because of the character of the heat transfer at the coolant-skin interface, correlation parameters were successfully found.

The heat flux entering the coolant from the skin and the Nusselt number along this interface are shown for the nominal turbulent-flow, water-cooled skin in figure 9. The Nusselt number has a large "plateau" value upstream of the heated region and a very small value downstream of the heated zone. This plateau behavior was observed in reference 6 and is explained as the result of the temperatures in the coolant being fully developed with an exponential variation of heat flux from the wall into the coolant. From the interface heat flux $\dot{q}_i$ (fig. 9), it is seen that over 70 percent of the heat enters the coolant when the Nusselt number is within 90 percent of the plateau value. Also, almost no heat enters the coolant when the Nusselt number is at the low downstream value. Similar behavior is found for every case in the parameter studies reported in this paper. Because of the relatively simple boundary conditions at the coolant-skin interface, the following approximate model of the steady-state conduction in the skin is suggested:

$$\frac{\partial^2 T}{\partial x^2} + \frac{\partial^2 T}{\partial y^2} = 0 \tag{A1}$$

with boundary conditions

$$-k_s \frac{\partial T}{\partial y} = \begin{cases} h_H(T - T_{\text{in}}) & (x < 0) \\ 0 & (x \geq 0) \end{cases} \tag{A2}$$

for $y = 0$, and

$$-k_s \frac{\partial T}{\partial y} = \begin{cases} \dot{Q} & (0 < x < w) \\ 0 & (\text{Otherwise}) \end{cases} \tag{A3}$$

for $y = -h_s$ where $h_H$ is the constant convective film coefficient derived from the plateau value of the Nusselt number.

In equations (A1) to (A3), the streamwise ($x$) extent of the solution domain is assumed to be infinite, and the origin of the $x$-axis is located at the position where the external skin is heated. To continue with the analysis, the following nondimensional terms are defined:

$$T^* = \frac{k_s(T - T_{\text{in}})}{\dot{Q} h_s} \tag{A4}$$

$$(x^*, y^*) = \frac{(x, y)}{h_s} \tag{A5}$$

$$\text{Bi} = \frac{h_s h_H}{k_s} \tag{A6}$$

where $T^*$ and $(x^*, y^*)$ are the nondimensional temperature and position coordinates, respectively, and Bi is the Biot number. With this nondimensionalization, equations (A1) to (A3) become

$$\frac{\partial^2 T^*}{\partial x^{*2}} + \frac{\partial^2 T^*}{\partial y^{*2}} = 0 \tag{A7}$$

and

$$-\frac{\partial T^*}{\partial y^*} = \begin{cases} \text{Bi } T^* & (x^* < 0) \\ 0 & (x^* \geq 0) \end{cases} \tag{A8}$$

for $y^* = 0$, and

$$-\frac{\partial T^*}{\partial y^*} = \begin{cases} 1 & (0 < x^* < w/h_s) \\ 0 & (\text{Otherwise}) \end{cases} \tag{A9}$$

for $y^* = -1$. This simplified conduction model suggests that the maximum nondimensional temperature in the skin is a function of only two parameters, Bi and $w/h_s$.

The results of the parametric studies for maximum skin temperature have been nondimensionalized and plotted against the Biot number for four values of $w/h_s$ in figure A1. All the curves that approximate the data points are essentially the same shape but are shifted in the figure. The value of the convective film coefficient $h_H$ used in the Biot number is taken at the streamwise location with the largest value of $\dot{q}_i$. These two parameters, Bi and $w/h_s$, correlate the data very well. The data for $w/h_s = 0.75$ are particularly informative, because they represent 48 cooling cases that consist of all three coolants, with both laminar and turbulent flow, and coolant property variations. Unfortunately, these results cannot be used to simplify

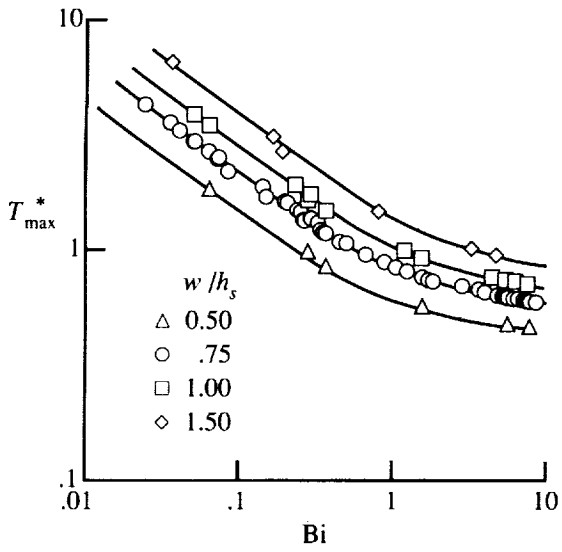


Figure A1. Variation of maximum nondimensional temperature with Biot number for several values of $w/h_s$.

the prediction of maximum skin temperatures because the plateau value of the convective film coefficient, which is used to determine the Biot number, can only be obtained from a numerical analysis as done in the present study.

## References


1. Wilhite, Alan W.; Powell, Richard W.; Scotti, Stephen J.; McClinton, Charles R.; Pinckney, S. Zane; Cruz, Christopher I.; Jackson, L. Robert; Hunt, James L.; Cerro, Jeffrey A.; and Moses, Paul L.: Concepts Leading to the National Aero-Space Plane Program. AIAA-90-0294, Jan. 1990.

2. Holden, M. S.; Wieting, A. R.; Moselle, J. R.; and Glass, C.: Studies of Aerothermal Loads Generated in Regions of Shock/Shock Interaction in Hypersonic Flow. AIAA-88-0477, Jan. 1988.

3. Nowak, Robert J.; Holden, Michael S.; and Wieting, Allan R.: Shock/Shock Interference on a Transpiration Cooled Hemispherical Model. AIAA-90-1643, June 1990.

4. Kasper, Harold J.: Thrust Chamber Life Prediction. *Advanced High Pressure $O_2/H_2$ Technology,* S. F. Morea and S. T. Wu, eds., NASA CP-2372, 1985, pp. 36–43.

5. Axcell, B. P.; Tonge, D. A.; and Jemsson, T.: Turbulent Forced Convection in a Pipe With an Exponential Wall Heat Flux. *Experimental Heat Transfer, Fluid Mechanics, and Thermodynamics—1988,* R. K. Shah, E. N. Ganić, and K. T. Yang, eds., Elsevier Science Publ. Co., Inc., 1988, pp. 808–815.

6. Reichardt, H.: *The Principles of Turbulent Heat Transfer.* NACA TM 1408, 1957.

7. Van Driest, E. R.: On Turbulent Flow Near a Wall. *Aeronaut. Sci.*, vol. 23, no. 11, Nov. 1956, pp. 1007–1011, 1036.

8. Petukhov, B. S.: Heat Transfer and Friction in Turbulent Pipe Flow With Variable Physical Properties. *Advances in Heat Transfer, Volume 6,* James P. Hartnett and Thomas F. Irvine, Jr., eds., Academic Press, Inc., 1970, pp. 503–564.

9. Kays, W. M.; and Crawford, M. E.: *Convective Heat and Mass Transfer,* Second ed. McGraw-Hill, Inc., c.1980.

10. Anderson, Dale A.; Tannehill, John C.; and Pletcher, Richard H.: *Computational Fluid Mechanics and Heat Transfer.* Hemisphere Publ. Corp., c.1984.

11. Beam, Richard M.; and Warming, R. F.: An Implicit Factored Scheme for the Compressible Navier-Stokes Equations. *AIAA J.*, vol. 16, no. 4, Apr. 1978, pp. 393–402.

12. Heaton, H. S.; Reynolds, W. C.; and Kays, W. M.: Heat Transfer in Annular Passages. Simultaneous Development of Velocity and Temperature Fields in Laminar Flow. *Int. J. Heat & Mass Transf.*, vol. 7, no. 7, July 1964, pp. 763–781.

13. Hatton, A. P.; and Quarmby, Alan: The Effect of Axially Varying and Unsymmetrical Boundary Conditions on Heat Transfer With Turbulent Flow Between Parallel Plates. *Int. J. Heat & Mass Transf.*, vol. 6, no. 10, Oct. 1963, pp. 903–914.

14. Goldberg, Fredric N.; and Haferd, Angela M.: *Numerical Procedures for Calculating Real Fluid Properties of Normal and Parahydrogen.* NASA TN D-4341, 1968.

15. Hendricks, Robert C.; Peller, Ildiko C.; and Baron, Anne K.: *WASP—A Flexible FORTRAN IV Computer Code for Calculating Water and Steam Properties.* NASA TN D-7391, 1973.

16. Boman, B. L.; Citrin, K. M.; Garner, E. C.; and Stone, J. E.: *Heat Pipes for Wing Leading Edges of Hypersonic Vehicles.* NASA CR-181922, 1990.

17. Touloukian, Y. S.; Saxena, S. C.; and Hestermans, P.: Viscosity. *Thermophysical Properties of Matter,* Volume 11, IFI/Plenum, c.1975.

18. Research and Advanced Projects Deps.: *Investigation of Cooling Problems at High Chamber Pressures—Final Report.* NASA CR-78634, 1966.

NASA
National Aeronautics and Space Administration

# Report Documentation Page

| 1. Report No. | 2. Government Accession No. | 3. Recipient's Catalog No. |
|---|---|---|
| NASA TP-3100 | | |

| 4. Title and Subtitle | 5. Report Date |
|---|---|
| Numerical Studies of Convective Cooling for a Locally Heated Skin | May 1991 |
| | 6. Performing Organization Code |
| 7. Author(s) | 8. Performing Organization Report No. |
| Stephen J. Scotti | L-16867 |
| 9. Performing Organization Name and Address | 10. Work Unit No. |
| NASA Langley Research Center<br>Hampton, VA 23665-5225 | 506-43-71-04 |
| | 11. Contract or Grant No. |
| 12. Sponsoring Agency Name and Address | 13. Type of Report and Period Covered |
| National Aeronautics and Space Administration<br>Washington, DC 20546-0001 | Technical Paper |
| | 14. Sponsoring Agency Code |

15. Supplementary Notes

16. Abstract

A computational study of the effectiveness of tangential convective cooling for the protection of structures from intense, localized thermal loads is presented. Two-dimensional numerical models of an idealized cooling problem are developed and validated. Detailed results and a parametric study of cooling effectiveness are presented for a thermal load representative of a shock-shock interaction on the engine cowl leading edge of a hypersonic study vehicle. The parameters investigated are flow conditions (laminar or turbulent), coolant type (liquid sodium, liquid water, or supercritical, cryogenic hydrogen), coolant mass-flow rate, extent of the heated region, thickness of the heated skin, and bulk properties of the coolant. The results indicate that for specific combinations of parameters, all three coolants may yield temperatures within the temperature limits of a copper-alloy, engine cowl leading edge. However, a liquid sodium coolant is the least sensitive of the three coolants to the assumed flow conditions and to the other parameters investigated in the study.

| 17. Key Words (Suggested by Author(s)) | 18. Distribution Statement |
|---|---|
| Convective cooling<br>Heat transfer | Unclassified—Unlimited<br><br>Subject Category 34 |

| 19. Security Classif. (of this report) | 20. Security Classif. (of this page) | 21. No. of Pages | 22. Price |
|---|---|---|---|
| Unclassified | Unclassified | 20 | A03 |

NASA FORM 1626 OCT 86

NASA-Langley, 1991

For sale by the National Technical Information Service, Springfield, Virginia 22161-2171